Interplay of disorder and antiferromagnetism in TlFe1.6+(Se1–xSx)2 probed by neutron scattering

S.J.E. Carlsson, David Santos-Cottin, Christophe Lepoittevin, Pierre Strobel,
Vivian Nassif, Emmanuelle Suard, Pierre Toulemonde

Interplay of disorder and antiferromagnetism in TlFe$_{1.6+\delta}$(Se$_{1−x}$S$_x$)$_2$ probed by neutron scattering

S J E Carlsson[1,2], D Santos-Cottin[1,2,3], Ch Lepoittevin[1,2], P Strobel[1,2], V Nassif[1,2], E Suard[4] and P Toulemonde[1,2]

[1] Université de Grenoble Alpes, Inst NEEL, F-38042 Grenoble, France
[2] CNRS, Inst NEEL, F-38042 Grenoble, France
[3] IMPMC, UPMC 4, Place Jussieu, 75005 Paris, France
[4] ILL, 71 Avenue des Martyrs, 38000 Grenoble, France

E-mail: sandra.karlsson@neel.cnrs.fr and pierre.toulemonde@neel.cnrs.fr

Abstract

The effect of selenium substitution by sulphur on the structural and physical properties of antiferromagnetic TlFe$_{1.6+\delta}$Se$_2$ has been investigated via neutron, x-ray and electron diffraction, and transport measurements. The $\sqrt{5}\,a \times \sqrt{5}\,a \times c$ super-cell related to the iron vacancy ordering found in the pure TlFe$_{1.6}$Se$_2$ selenide is also present in the S-doped TlFe$_{1.6+\delta}$(Se$_{1−x}$S$_x$)$_2$ compounds. Neutron scattering experiments show the occurrence of the same long range magnetic ordering in the whole series i.e. the 'block checkerboard' antiferromagnetic structure. In particular, this is the first detailed study where the crystal structure and the $\sqrt{5}\,a \times \sqrt{5}\,a$ antiferromagnetic structure is characterized by neutron powder diffraction for the pure TlFe$_{1.6+\delta}$S$_2$ sulphide over a large temperature range. We demonstrate the strong correlation between occupancies of the crystallographic iron sites, the level of iron vacancy ordering and the occurrence of block antiferromagnetism in the sulphur series. Introducing S into the Se sites also increases the Fe content in TlFe$_{1.6+\delta}$(Se$_{1−x}$S$_x$)$_2$ which in turn leads to the disappearance of the Fe vacancy ordering at $x = 0.5 \pm 0.15$. However, by reducing the nominal Fe content, the same $\sqrt{5}\,a \times \sqrt{5}\,a \times c$ vacancy ordering and antiferromagnetic order can be recovered also in the pure TlFe$_{1.6+\delta}$S$_2$ sulphide with a simultaneous reduction in the Néel temperature from 435 K in the selenide TlFe$_{1.75}$Se$_2$ to 330 K in the sulphide TlFe$_{1.5}$S$_2$. The magnetic moment remains high at low temperature throughout the full substitution range, which contributes to the absence of superconductivity in these compounds.

Keywords: iron-based superconductors, neutron powder diffraction, crystallography, magnetism, chalcogenides

(Some figures may appear in colour only in the online journal)

1. Introduction

The discovery of bulk superconductivity in A$_{1−y}$Fe$_{2−z}$Se$_2$ (A = K, Cs, Rb, Tl) with a T_C of about 30 K generated a lot of interest because of the coexistence of magnetic order and superconductivity [1–4]. The closely related TlFe$_{2−z}$Se$_2$ was first studied by Häggström *et al* [5] 25 years ago and crystallizes in a ThCr$_2$Si$_2$-type structure (with a $a \times a \times c$ tetragonal lattice, space group I4/*mmm*) with possible ordering of the vacancies in the Fe layer. A $\sqrt{5}\,a \times \sqrt{5}\,a$ ordering in the iron planes occurs when z is equal to 0.4 i.e. for 20% iron vacancies and is formed through modulating of the Fe deficiency in the Fe-Se layer by the formation of Fe ions in 16*i* positions (Fe1) and empty Fe sites in 4*d* positions (Fe2). Other types of vacancy ordering have also been reported in sulphides in the past e.g. the $a\sqrt{2} \times 2a\sqrt{2} \times c$ orthorhombic cell found for 25% (z = 0.5) iron vacancies [6].

In $TlFe_{1.6}Se_2$ single crystals, vacancy ordering occurs below ~460 K and bulk c-axis antiferromagnetism is found below T_N ~ 430 K [7]. Often, the vacancy order is incomplete with partial occupancies observed on at least one of the Fe sites. Whereas $TlFe_{1.6}Se_2$ is a Mott-insulator [8, 9], superconductivity with a T_C ~ 20 K was observed for $z = 0.3$ i.e. $TlFe_{1.7}Se_2$. However, the shielding volume fraction was very small (<1%) and the corresponding superconducting phase was not identified [4]. In alkaline selenides, the superconducting samples are defined by a nano-scale phase separation and the full characteristics of the superconducting phase are still uncertain. Different hypotheses have been reported in the literature: A strongly alkaline deficient intercalated phase ($Rb_{0.3}Fe_2Se_2$ [10]), a 1/8 Fe vacancy state [11], a vacancy free phase (AFe_2Se_2 [12, 13]) or a disordered Fe vacancy phase [14]. As a consequence, pure Tl based selenides, which are more stable in air than alkaline intercalated selenides, without additional disorder on the A-site are interesting systems to study to better understand the interplay between the Fe vacancy ordering, the magnetic order and superconductivity.

In iron-based superconductors, such as $BaFe_2(As_{1-x}P_x)_2$ and $Fe_{1+\delta}Te_{1-x}Se_x$, superconductivity can be induced or enhanced by simple isovalent substitution of the pnictogen or chalcogen [15–18]. Isovalent substitution can also suppress the superconductivity, as in a recent investigation by Lei *et al*, of the potassium intercalated $K_{1-y}Fe_{2-z}(Se_{1-x}S_x)_2$ ($T_C = 33$ K for $x = 0$) where increasing the sulphur content led to the disappearance of the superconductivity for $x \sim 0.8$ [19]. They suggest that this may be related to a decrease in the number of Fe vacancies or increased $FeCh_4$ tetrahedron distortion. Following this, we synthesized the full solid solution series of $Tl_{1-y}Fe_{2-z}(Se_{1-x}S_x)$ and found that increased sulphur substitution leads to a reduction in the Néel temperature, directly related to the Fe-Se/S bond length decrease but no superconductivity was found down to 4.2 K [20]. In this work, the crystal and magnetic structure and electrical transport of polycrystalline $TlFe_{1.6+\delta}(Se_{1-x}S_x)_2$ ($\delta <$ 0.1) samples as a function of temperature and sulphur substitution are further investigated using neutron powder diffraction (NPD). To our knowledge, this is the first time that sulphur-rich compositions, including the pure sulphide, have been studied by neutron scattering over a large temperature range.

2. Experimental methods

Polycrystalline samples of $TlFe_{1.6+\delta}(Se_{1-x}S_x)_2$ ($\delta = 0$ refers to the perfect $\sqrt{5}\,a\times\sqrt{5}\,a\times c$ ordered lattice) were prepared by a sealed tube technique similar to that reported elsewhere for $Fe_{1-\delta}(Te_{1-x}Se_x)$ [21, 22]. Starting materials were Fe powder (Alfa Aesar, 99.98%), Tl pieces (Alfa Aesar, 99.99%), Se chips (Alfa Aesar, 99.999%), FeS powder (Alfa, 99.9%) and S powder (Prolabo, 99.9%). Nominal mixtures of the reactants corresponding to $TlFe_{1.75}(Se_{1-x}S_x)_2$, total mass of elements ~2 g, were placed in alumina crucibles and sealed in evacuated silica tubes and heated at 100 °C h^{-1} up to 350 °C. After 24 h, the temperature was increased at 100 °C h^{-1} to 700 °C and kept there for 12 h. The samples where then cooled down to 350 °C, maintained at this temperature for 48 h, before being furnace cooled. The phase purity of the resulting powders was examined by x-ray powder diffraction using Cu Kα radiation.
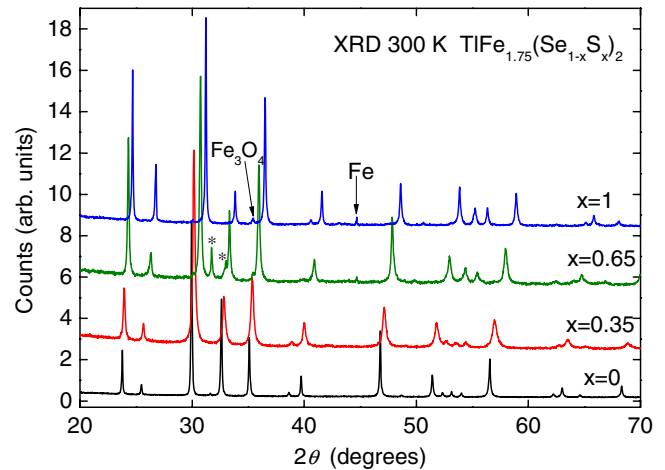

Figure 1. Powder XRD patterns of $TlFe_{1.75}(Se_{1-x}S_x)_2$ (nominal compositions) at 300 K with the position of the main impurity diffraction peaks marked as Fe_3O_4, Fe and * (unknown).

Neutron powder diffraction was used to study the structural and magnetic phase transitions in $TlFe_{1.6+\delta}(Se_{1-x}S_x)_2$ with $x = 0$, 0.35, 0.65 and 1.0. Low temperature measurements were carried out between 1.5 and 300 K with the D1B diffractometer at Institut Laue Langevin (ILL, Grenoble) using a monochromatic beam with $\lambda = 2.52$ Å. This was followed by a second experiment performed on the high-resolution diffractometer D2B at the ILL in the temperature range 5–470 K. The instrument was used in the high-resolution mode with a wavelength of $\lambda = 1.594$ Å (from the Ge(335) reflection of the monochromator). All the diffraction data were analyzed by the Rietveld method [23] using the GSAS [24] program suite.

Low temperature powder x-ray diffraction data were collected between 5 and 300 K using a Bruker D8 diffractometer working in the reflection mode at the wavelength $\lambda = 1.54$ Å and an ARS cooling system. Rietveld refinements of the data were performed with the FULLPROF package [25]. Data points with $10° \leq 2\theta \leq 90°$ were taken into account and pseudo-Voigt profile shape was used. The background was fitted using a linear interpolation between selected points.

Electron diffraction (ED) and quantitative energy dispersive spectroscopy (EDS) analysis were performed using a Philips CM 300ST transmission electron microscope (TEM) operating at 300 kV. Specimens were prepared by crushing a small piece of sample in an agate mortar under ethanol. A droplet of this mixture was then dropped on a copper grid covered by a holey carbon film.

The DC electrical resistivity of the samples was measured by a standard four-point contact technique in the temperature ranges 4.2–300 K and 280–570 K using two different experimental set-ups.

3. Results and discussion

3.1. Effect of S doping on the structural and physical properties of $TlFe_{1.6+\delta}(Se_{1-x}S_x)_2$

The x-ray powder diffraction patterns of the $TlFe_{1.75}(Se_{1-x}S_x)_2$ samples with $x = 0$, 0.35, 0.65 and 1 (nominal) collected at 300 K are presented in figure 1. Rietveld analysis of the data

Table 1. Refined structural parameters for $TlFe_{1.6+\delta}(Se_{1-x}S_x)_2$ ($x = 0$, 0.35, 0.65 and 1) from neutron diffraction data (D2B) collected at 300 K.

Atom	Par	$x = 0$	$x = 0.35$	$x = 0.65$	$x = 1$
	a (Å)	8.6852(3)	8.5956(5)	3.7916(3)	3.7444(2)
	c (Å)	13.9820(5)	13.826(1)	13.537(2)	13.3189(7)
Tl1	n	1	1	1	0.901(6)
Tl2	x	0.204(2)	0.195(3)		
	y	0.394(2)	0.394(3)		
	n	1	1		
Fe1 (16i)	x	0.094(1)	0.099(2)		
	y	0.198(1)	0.196(2)		
	z	0.2430(4)	0.2408(5)		
	n	0.861(9)	0.894(13)		
	Mz (μ_B)	1.82(5))	1.65(7)		
Fe2 (4d)	n	0.31(3)	0.52(4)	0.877(10)	0.832(6)
Se1/S1	z	0.365(1)	0.373(1)	0.3532(4)	0.3509(4)
	n	1/0	1/0	0.407(16)/ 0.593(16)	0/1
Se2/S2	x	0.198(2)	0.197(2)		
	y	0.394(1)	0.393(2)		
	z	0.3541(3)	0.3521(4)		
	n	1	0.68(3)/ 0.32(3)		
	Rp (%)	2.29	5.77	5.67	7.11
	Rwp (%)	3.06	7.36	7.32	8.90
	RF^2	11.04	7.24	7.45	13.07
	χ^2	2.85	3.95	3.881	2.684
	Fe_3O_4 (%)	0	2.2(1)	0.97(17)	5.2(3)
	Fe (%)	0	2.50(8)	3.27(8)	2.1(1)
	Refined Compos.	$TlFe_{1.5(1)}Se_2$	$TlFe_{1.6(1)}Se_{1.5(1)}S_{0.5(1)}$	$TlFe_{1.7(1)}Se_{0.8(1)}S_{1.2(1)}$	$Tl_{0.9(1)}Fe_{1.7(1)}S_2$

Space group $I4/m$ ($x = 0$ and 0.35) with atomic positions Tl1, 2a (0,0,0), Tl2 8h (x,y,0), Fe1 16i (x,y,z), Fe2 4d (0,1/2,1/4), Se1 4e (0,0,z) and Se2 16i (x,y,z). A magnetic model with $I4/m$' with only the Mz component was used for the fitting. Space group $I4/mmm$ ($x = 0.65$ and 1) with atomic positions Tl1, 2a (0,0,0), Fe2 4d (0,1/2,1/4) and Se1 4e (0,0,z).

showed that the $TlFe_{1.6+\delta}Se_2$ compound is pure whereas the S substituted samples contain small amounts (less than 6%) of Fe_3O_4 and Fe. The $x = 0.65$ pattern also have two additional diffraction peaks from some unknown impurity. All the diffraction peaks belonging to the main $TlFe_{1.6+\delta}(Se_{1-x}S_x)_2$ phase could be indexed in the tetragonal $ThCr_2Si_2$ structure, space group $I4/mmm$, found in the $AeFe_2As_2$ (Ae = Ba, Sr, Ca) arsenides and also used originally for the superconducting $K_{1-y}Fe_{2-z}Se_2$ [1]. The super-lattice reflections associated with the $I4/m$ symmetry ($\sqrt{5} a \times \sqrt{5} a \times c$), that includes a Fe ordered vacancy site, are difficult to detect in the XRD patterns because of their very low relative intensities.

EDS analysis carried out in a TEM on several crystallites of the pure selenide ($x = 0$) compound showed that the average Fe content was 1.6(1), in agreement with the Rietveld calculations (table 1). The electron diffraction patterns reveal a body-centred tetragonal subcell with the parameters $a = b \approx 3.9$Å, $c \approx 14$Å and extinction conditions compatible with the $I4/mmm$ space group (figure 2(a)). However, additional reflections i.e. satellite reflections, are also visible in the [001]-oriented basal plane (figure 2(b)). These are characteristic of a modulated structure that can be described by a two-component modulation vector. Two vectors can be defined: one along the [210]* direction and another one along the [$\bar{1}$20]* direction of the subcell, with an amplitude of 1/5, leading to the values $\vec{q_1^*} = 1/10(-2\vec{a^*} + 4\vec{b^*})$ and $\vec{q_2^*} = 1/10(4\vec{a^*} + 2\vec{b^*})$. Bearing in mind the commensurate nature of the modulation, the structure can also be described in the tetragonal supercell $a_{SC} = b_{SC} \approx 8.7$Å (= $\sqrt{5} a$), $c \approx 14$Å (space group $I4/m$). This result is in agreement with our neutron diffraction data, which shows evidence of the $\sqrt{5} a \times \sqrt{5} a \times c$ supercell, previously reported

for the insulating and antiferromagnetic (AFM) phases of the $Cs_{1-y}Fe_{2-z}Se_2$ and the $K_{1-y}Fe_{2-z}Se_2$ systems [26–28].

The ED analysis also verifies the ordering of the Fe vacancies, in particular for $x = 0$. The HRTEM image displayed in figure 2(c) was taken with the beam parallel to the [001] direction (with the simulated image on the inset). In this orientation the Fe vacancies are aligned in columns parallel to the electron beam and can be seen as bright spots (corresponding to weak electron density zones). The distance measured between the spots is ~9Å, corresponding to the $a_{SC} = b_{SC}$ (= $\sqrt{5} a$) lattice parameter and hence, to the distance between the Fe2 vacancy sites in the crystal structure. The [001]-projected structure is superimposed on the HRTEM image to highlight the tetragonal $\sqrt{5} a \times \sqrt{5} a$ unit cell.

The electrical resistance measured in the temperature range 5–600 K for the $TlFe_{1.75}(Se_{1-x}S_x)_2$ (nominal composition) samples are presented in figure 3. All compounds show typical semiconducting behaviour at low temperature, independent of the sulphur content. No superconductivity was found down to 5 K as already observed in our previous study of $Tl_{0.8}Fe_{1.5}(Se_{1-x}S_x)_2$ (nominal composition [20]). At high temperature, the anomaly associated with the AFM transition is clearly visible in the compositions $x = 0$ and $x = 0.35$ at $T_N = 435$ K and 390 K, respectively. The same kind of anomaly was observed in the alkaline-based $A_{1-y}Fe_{2-z}Se_2$ system [29, 30]. A gradual decrease of T_N with increased S content was observed in our previous $Tl_{1-y}Fe_{2-z}(Se_{1-x}S_x)_2$ series with $T_N = 435(15)$ K for $x = 0$ and 330(5) K for $x = 1$ [20]. However, in this study there is no visible anomaly in the resistivity curve of the $x = 0.65$ and $x = 1$ compositions, confirming the absence of long-range magnetic ordering for these samples. This is in
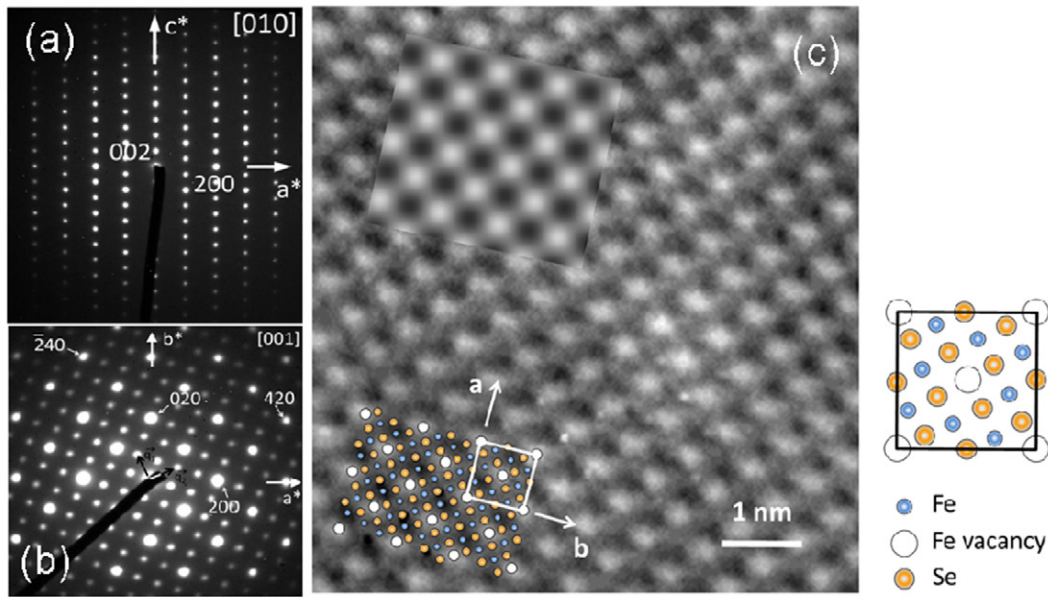
Figure 2. Zone axis electron diffraction patterns of $TlFe_{1.6+\delta}Se_2$ recorded along (*a*) the [010] and (*b*) the [001] directions. On the later satellites reflections define two possible modulation vectors $\vec{q_1}$ and $\vec{q_2}$. (*c*) [001] HRTEM image of $TlFe_{1.6+\delta}Se_2$ recorded for a defocus value of -57 nm with the corresponding simulated image (top left corner) and the structure projected along the $\vec{c}$ parameter with the squared basal plane of the tetragonal supercell.

agreement with the neutron diffraction data at 300 K which confirms that the $(101)_M$ magnetic peak, associated with the AFM phase in the $\sqrt{5}\,a\times\sqrt{5}\,a\times c$ lattice, is present in $TlFe_{1.75}Se_2$ and $TlFe_{1.75}(Se_{0.65}S_{0.35})_2$ but absent in $TlFe_{1.75}(Se_{0.35}S_{0.65})_2$ and $TlFe_{1.75}S_2$ (figure 4(*a*)). Neutron diffraction data were also collected on cooling from 300 to 1.7 K (figures 4(*b*), (*c*)). They show that the $(101)_M$ magnetic peak remains down to 1.7 K in both the $x = 0$ and $x = 0.35$ samples. However, whereas the magnetic moment in the pure selenide ($x = 0$) reaches a clear maximum at ~180 K and then slowly diminishes as the temperature is reduced (figure 4(*b*)), the moment in the $x = 0.35$ compound appear to peak at ~100 K and then remains almost constant down to the lowest measured temperature (figure 4(*c*)). In $TlFe_{1.75}(Se_{0.65}S_{0.35})_2$, the refined magnetic moment increases from 1.65(7) μ_B at 300 K to 2.21(9) μ_B at 1.5 K.

Figure 5 illustrates the refined structural parameters of $TlFe_{1.6+\delta}(Se_{1-x}S_x)_2$ as a function of S substitution at room temperature (RT), based on XRD and NPD data. The unit cell parameters of $TlFe_{1.6+\delta}(Se_{1-x}S_x)_2$ slowly decrease as a function of increased S substitution (figure 5(*a*)), indicating that the smaller sulphur atom is being incorporated into the structure. The gradual contraction of the lattice with S doping can also be seen in the neutron powder diffraction data as a shift of the (110) and (002) peak positions to a higher angle (figure 4(*a*)). The absence of any superstructure reflections (in particular those of the $\sqrt{5}\,a\times\sqrt{5}\,a\times c$ lattice) in the $x = 0.65$ and 1.0 neutron diffraction patterns at RT indicate an order-disorder transition in the present $TlFe_{1.75}(Se_{1-x}S_x)_2$ series for high sulphur content. Hence, keeping the nominal Fe content at 1.75 for $x > 0.35$ compositions, produces samples with disordered iron vacancies, as described in the $I4/mmm$ space group.
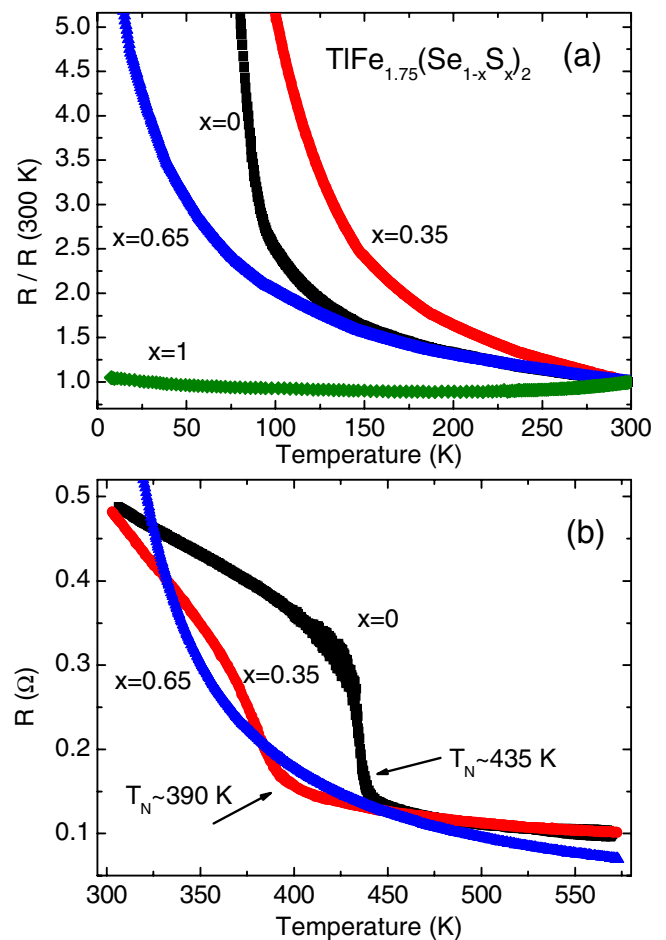

Figure 3. Temperature dependence of the electrical resistance, $R(T)$, for $TlFe_{1.75}(Se_{1-x}S_x)_2$ polycrystalline samples (nominal compositions) with $x = 0$, 0.35 and 0.65 below (*a*) and above (*b*) room temperature.
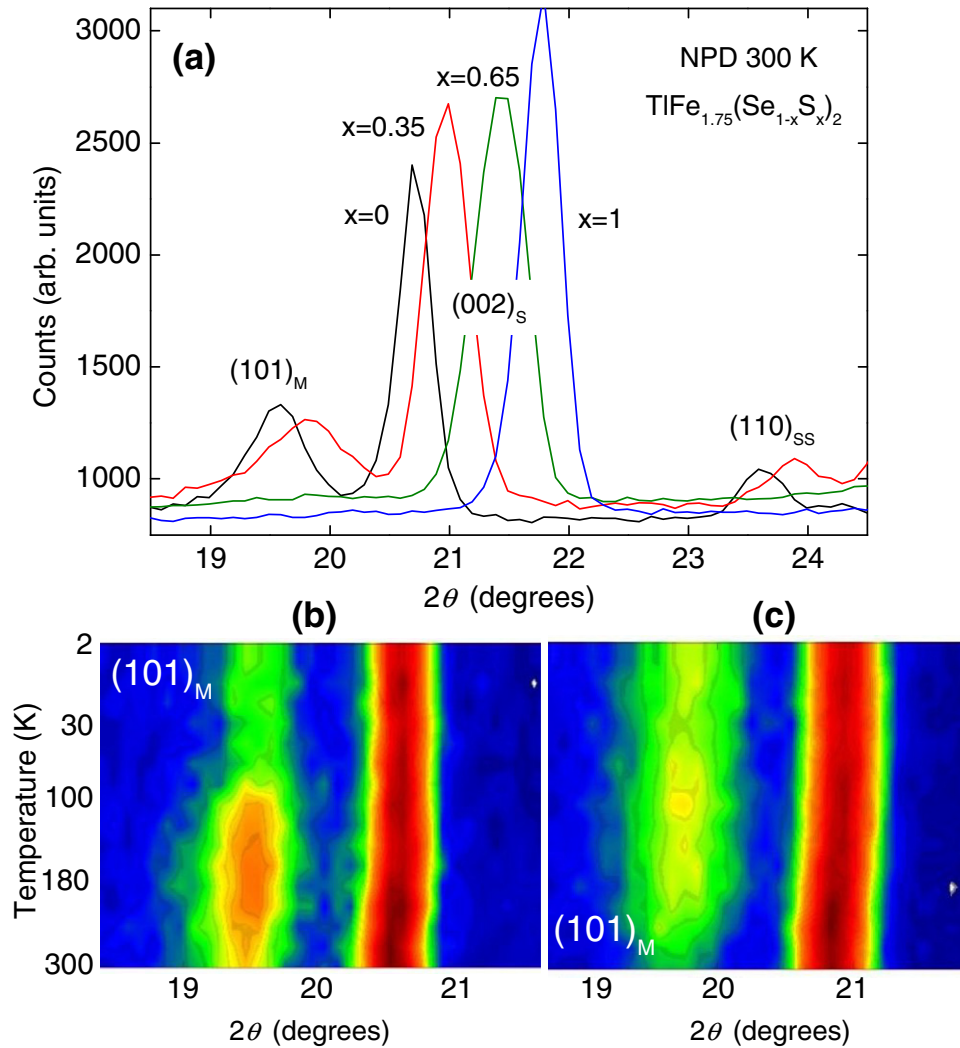
Figure 4. Portion of the neutron powder diffraction patterns (D1B) of $TlFe_{1.75}(Se_{1-x}S_x)_2$ samples (nominal compositions) collected at 300 K showing the changes in the (101) magnetic peak, the (002) structural peak, and the (110) super lattice peak with different S content, *x*. (*a*) and on cooling from 300 to 1.7 K showing the changes in intensity of the (101) magnetic peak with temperature for the $x = 0$ and $x = 0.35$ samples (*b* and *c*).

Whereas the lattice parameters decrease continuously with S content at RT (figure 5(*a*)), the variations of the Fe-Se/S height and bond distances (figures 5(*b*), (*c*)) are irregular, confirming that there are two different regimes, above and below the $x = 0.5 \pm 0.15$ composition. This was also observed by Lei *et al* in their $K_{1-y}Fe_{2-z}(Se_{1-x}S_x)_2$ series where the structural parameters and the real iron content show a discontinuity in their variations at $x = 0.5$ [19].

The refined structural parameters for $TlFe_{1+\delta}(Se_{1-x}S_x)_2$ ($x = 0$, 0.35, 0.65 and 1) from NPD data (D2B) are listed in table 1. The total refined Fe content in the Fe-Se/S lattice increases gradually with the nominal S content: 1.5, 1.6, and 1.7 in $x = 0$, 0.35 and 0.65 and 1 respectively (inset figure 5(*c*)). This is also the case for $KFe_{2-z}(Se_{1-x}S_x)_2$ studied by Lei *et al* [19]. On the Fe2 site, which should be empty in a fully ordered $\sqrt{5}a \times \sqrt{5}a \times c$ $TlFe_{1.6}Ch_2$ (Ch = Se, S) phase, the occupancy goes from 0.31 to 0.52 between the $x = 0$ and 0.35 samples, explaining why the perfect vacancy ordering, and hence the magnetic order, is lost as the S content increases above $x = 0.35$. On the other hand, the occupancy

on the almost fully occupied Fe1 site does not seem to be affected by the S doping.

Bearing in mind the fact that neutron powder diffraction measures the average structure only, and that we observe signatures of long range magnetic order in our different measurements, we believe that our samples contain a major fraction crystallized in the $\sqrt{5}a \times \sqrt{5}a \times c$ lattice, which is well ordered with nearly no iron atoms on the Fe2 sites, and a second fraction where the Fe2 sites are probably filled above 50%. This effect is more important for the sulphur rich compositions i.e. $x = 0.65$ and $x = 1.0$, for which the well-ordered part of the sample is decreased to nearly zero (as we do no see any anomaly in R(T) curve at high T). In the following sections we focus our discussion on the pure selenide ($x = 0$) and sulphide ($x = 1$) compounds.

3.2. Temperature dependence of the structural and physical properties of $TlFe_{1.6+\delta}Se_2$

Powder neutron diffraction measurements were used to study both the crystal and magnetic structures of the pure $TlFe_{1.6+\delta}Se_2$

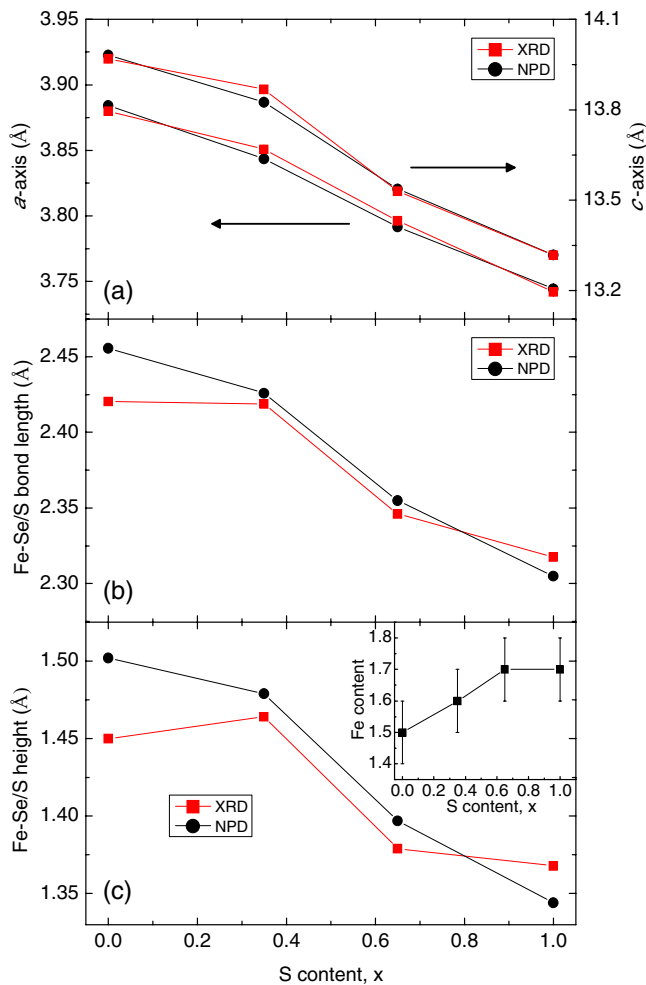**Figure 5.** (*a*) Refined lattice parameters (from Rietveld refinements of NPD and XRD data using the *I*4/*mmm* space group) of TlFe$_{1.75}$(Se$_{1-x}$S$_x$)$_2$ samples (nominal compositions) at 300 K as a function of the S content, *x*. (*b*) Fe-Se/S bond length and (*c*) height. Error bars are smaller than the symbols. Inset: variation of the refined Fe content with S substitution.

selenide in the temperature range 5–470 K. The refined structural parameters for TlFe$_{1.75}$Se$_2$ based on neutron powder diffraction data collected at 5, 150, 300, 390 and 470 K are listed in tables 2 and 3.

3.2.1. Low temperature behaviour. In the diffraction patterns collected between 5 and 390 K the (110) superlattice and (101) magnetic reflections associated with the tetragonal $\sqrt{5}\,a \times \sqrt{5}\,a \times c$ superstructure are present, in agreement with the ED study. Both the nuclear and magnetic structures were therefore refined together as one phase using the *I*4/*m* space group symmetry with a magnetic model of *I*4/*m*' (figure 6(*a*)). The Fe moments lie along the c-axis, aligned antiferromagnetically between layers in a 'blocked checkerboard' arrangement (Inset figure 6(*a*)) as previously reported for K$_{0.8}$Fe$_{1.6}$Se$_2$ [31]. The resulting magnetic moments of 1.83(4) μ_B at 300 K, 2.25(7) μ_B at 150 K and 1.78(8) μ_B at 5 K are lower than the moment of 3.2–3.4 μ_B observed at ~10 K in $\sqrt{5}\,a \times \sqrt{5}\,a \times c$ AFM A$_{0.8}$Fe$_{1.6}$Se$_2$ (A = K, Rb [28, 31]). However, they are all in good agreement with those reported for partially disordered

single crystals of TlFe$_{1.6}$Se$_2$ (1.72(6) μ_B at 300 K, 2.07(9) μ_B at 140 K, and 1.31(8) μ_B at 5 K [7]). For single crystal TlFe$_{1.6}$Se$_2$ with complete vacancy ordering, the magnetic moment reaches ~3 μ_B at 140 K (moment lying along the *c*-axis) and 5 K (moments lying in the $\sqrt{5}\,a \times \sqrt{5}\,a$ plane [32].

In partially disordered TlFe$_{1.6}$Se$_2$ single crystals, a canting of the magnetic moments between 100 and 150 K leads to an abrupt increase in the *c* lattice parameter of ~ 0.05–0.1 Å on cooling (although the effect is less visible in powdered samples obtained from these crystals, ~0.01 Å [33]). In contrast, in fully ordered TlFe$_{1.6}$Se$_2$ single crystals, the magnetic transition at 100 K i.e. the spin re-orientation from the *c*-axis into the *ab* plane is not associated with such anomaly [32]. The lattice parameters of our TlFe$_{1.6+\delta}$Se$_2$ sample, derived from low temperature XRD data (in agreement with the variation obtained from NPD) are shown in figures 7(*a*), (*b*). The behaviour of *c* is smooth around 100 K with no evidence of an increase in the *c*-axis, indicating that our TlFe$_{1.6+\delta}$Se$_2$ powder sample is rather well-ordered and homogenous.

The neutron diffraction data collected at 5 K on TlFe$_{1+\delta}$Se$_2$ powder were also refined using the non-collinear magnetic structure (magnetic space group *I*4/*m* with the moments lying in the $\sqrt{5}\,a \times \sqrt{5}\,a$ plane) used by May *et al* to model the magnetic structure of fully ordered TlFe$_{1.6}$Se$_2$ single crystals [32]. This resulted in a lower quality fit and a reduced magnetic moment of 1.4(1) μ_B, compared to 1.78(8) μ_B for the model with the moments lying along *c*. Hence, our results are in agreement with the findings by May *et al* which show that, in the magnetic ground state for partially disordered TlFe$_{1.6}$Se$_2$, the magnetic moments are aligned along the *c*-axis, and in fully ordered TlFe$_{1.6}$Se$_2$ they are lying in the *ab* plane [32].

Figure 8 shows the electrical resistance data for TlFe$_{1.6+\delta}$Se$_2$ between 5 and 500 K. Around 93 K there is a sharp increase in the resistivity with decreasing temperature and the resistance continues to increase down to ~13 K where it exceeds the limit of the instrument with a resistance of >2×10^5 Ω. Anomalies at around 100 K have also been observed in resistivity, magnetization and specific heat capacity measurements of both partially and fully ordered TlFe$_{1.6}$Se$_2$ single crystals, and were shown to be related to the spin re-orientation of the magnetic moments described before [7, 32]. In partially disordered TlFe$_{1.6}$Se$_2$ crystals a second anomaly can be seen in the resistivity data of Sales *et al* [7] at ~40 K related to a canting of the magnetic moments between 100 and 140 K [33]. In fully ordered crystals this magnetic transition at ~140 K is not visible in the resistivity nor in the magnetization data. Only the spin re-orientation transition at 100 K is visible in the *R*(T) and magnetic susceptibility curves. We do not see any anomaly in our resistivity data at 140 K. This is again an indication that the degree of ordering of our TlFe$_{1.6+\delta}$Se$_2$ powder sample is probably better than in the partially ordered crystals grown by Sales *et al* [7].

3.2.2. High temperature behaviour. In the NPD patterns acquired above RT we observed that, at 470 K the superlattice and magnetic reflections have disappeared as a result of the disorder of the Fe vacancies associated with the phase

Table 2. Refined structural parameters for $TlFe_{1.6+\delta}Se_2$ from neutron diffraction data (D2B) collected at 5, 150, 300 and 390 K.

	Par	5 K	150 K	300 K	390 K
	a (Å)	8.6299(2)	8.6532(4)	8.6852(3)	8.7040(7)
	c (Å)	13.9418(5)	13.954(1)	13.9820(5)	13.998(1)
Tl1	n	1	1	1	1
Tl2	x	0.199(2)	0.199(3)	0.204(2)	0.208(5)
	y	0.399(2)	0.340(3)	0.394(2)	0.403(5)
	n	1	1	1	1
Fe1 (16i)	x	0.098(2)	0.095(2)	0.094(1)	0.092(2)
	y	0.200(2)	0.200(2)	0.198(1)	0.201(3)
	z	0.2426(5)	0.2422(5)	0.2430(4)	0.244(1)
	n	0.89(2)	0.88(1)	0.861(9)	0.82(2)
	Mz (μ_B)	1.78(8)	2.25(7)	1.83(4)	1.2(1)
Fe2 (4d)	n	0.46(3)	0.44(8)	0.31(3)	0.38(7)
Se1	z	0.3804(9)	0.376(1)	0.365(1)	0.373(2)
	n	1	1	1	1
Se2	x	0.196(2)	0.196(2)	0.198(2)	0.198(4)
	y	0.397(2)	0.398(2)	0.394(1)	0.393(3)
	z	0.3542(2)	0.3545(3)	0.3541(3)	0.3522(5)
	n	1	1	1	1
	Rp (%)	3.28	2.89	2.29	2.60
	Rwp (%)	4.32	3.77	3.06	3.29
	RF^2	11.28	12.56	11.04	17.22
	χ^2	3.58	2.73	2.85	1.57

Space group $I4/m$ with atomic positions Tl1, *2a* (0,0,0), Tl2 *8h* (x,y,0), Fe1 *16i* (x,y,z), Fe2 *4d* (0,1/2,1/4), Se1 *4e* (0,0,z) and Se2 *16i* (x,y,z). A magnetic model with $I4/m'$ with only the Mz component was used for the fitting.

Table 3. Refined structural parameters for $TlFe_{1.6+\delta}Se_2$ at 470 K. Space group $I4/mmm$ with $a = 3.9073(4)$ Å and $c = 13.970(2)$ Å.

Atom	site	x	y	z	n
Tl	2a	0	0	0	1
Fe	4d	0	1/2	1/4	0.72(1)
Se	4e	0	0	0.3550(3)	1

$Rp = 2.68\%$, $Rwp = 3.39\%$, and $\chi^2 = 1.62$

transition from the $\sqrt{5}\,a \times \sqrt{5}\,a \times c$ (space group $I4/m$) to the $a \times a \times c$ $I4/mmm$ symmetry (figure 6(*b*)).

Figures 7(*a*), (*b*) shows the variation of the lattice parameters (expressed in the $a \times a \times c$ lattice) with temperature derived from the NPD and XRD data. Above the magneto-structural phase transition at ~430 K (see R(T) curve figure 8) there is a large increase in the *a*-axis and a change in the slope of the *a*(T) curve. Furthermore, the *c*-axis decreases sharply (0.03 Å) above the transition temperature. This effect was also observed in single crystals of $Cs_{0.83}Fe_{1.71}Se_2$ by Pomjakushin *et al* [26] and $TlFe_{1.6}Se_2$ by Cao *et al* [33]. For the latter compound, the reduction in *c* at high T is less pronounced, possibly due to the samples being less well ordered than the one used in our study. A substantial change in the lattice parameters across the AFM transition at ~435 K indicates a strong magnetoelastic coupling in these $A_{1-y}Fe_{1.6+\delta}Se_2$ (A = Tl, K, Rb, Cs) compounds.

Above RT the electrical resistance continuously decreases up to ~435 K where there is a steeper drop and above this temperature it decreases further but at a slower rate. This anomaly, as described in section A, is close to the Néel temperature, T_N ~ 430 K, observed in $TlFe_{1.6}Se_2$ by Sales *et al* [7] and can therefore be assumed to be associated with the antiferromagnetic transition. Comparing the heating and cooling R(T) curves between 300 and 570 K, the anomaly is observed at the same temperature ~435 K but there is clear hysteresis. After heating the sample up to 570 K, the room temperature resistance was
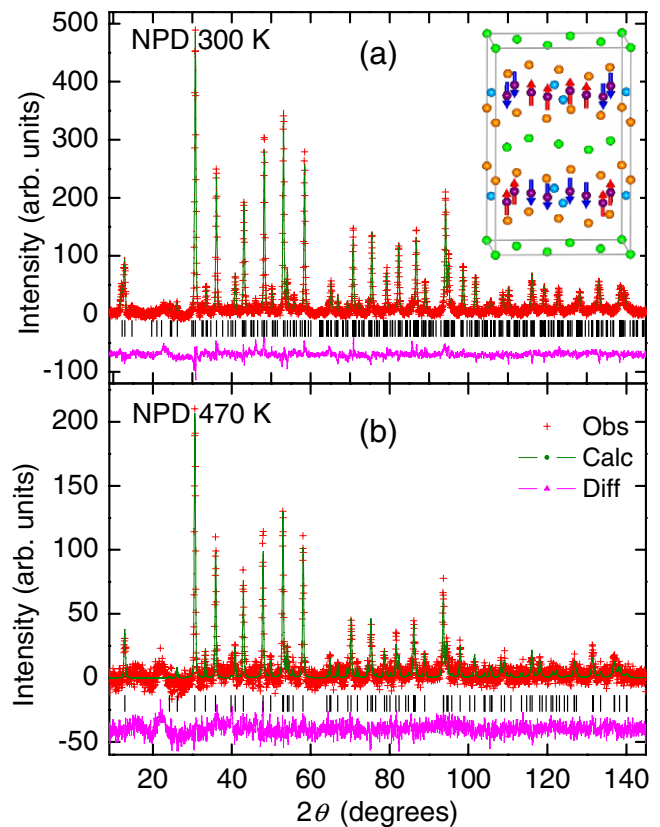

Figure 6. Rietveld refinement results for the neutron powder diffraction measurements (D2B) on $TlFe_{1.6+\delta}Se_2$ at 300 K and 470 K. Black ticks mark the Bragg peak positions. (*a*) The fit at 300 K was made using space group $I4/m$ with an antiferromagnetic ordering described by $I4/m'$. (*b*) The pattern at 470 K, where both the Fe vacancies and the magnetic moments are disordered, can be described by the tetragonal $ThCr_2Si_2$ structure, space group $I4/mmm$. Inset: crystal and magnetic structure of $TlFe_{1.6+\delta}Se_2$ in a tetragonal $I4/m$ unit cell with the occupied Fe1 sites marked dark purple, vacant Fe2 sites light blue, Se sites orange and Tl sites green.
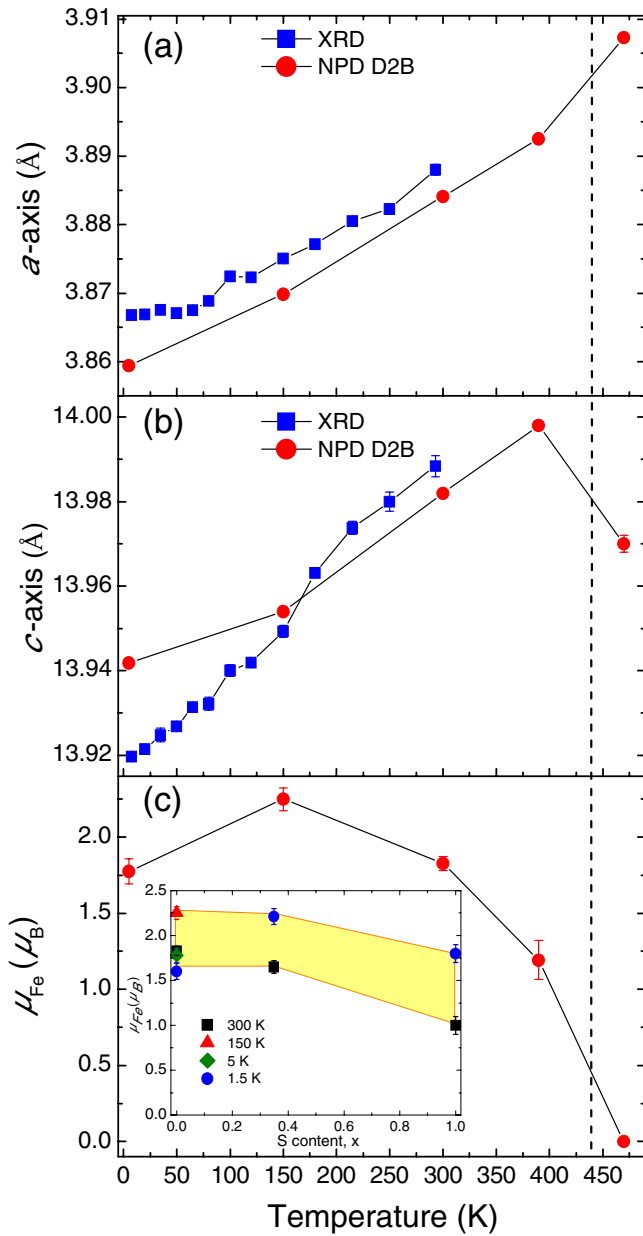
Figure 7. (*a*) and (*b*) Unit cell parameters of $TlFe_{1.6+\delta}Se_2$ as a function of temperature based on NPD and XRD data. (*c*) The refined magnetic moment (D2B data). Inset graph: the refined magnetic moment as a function of S content at various temperatures. The dashed line indicates T_N estimated from the R(T) measurements.

reduced by half implying that the phase transition is not fully reversible and that the Fe vacancy ordering is improved by this annealing. A structural study of $Cs_{0.83}(Fe_{1-y}Se)_2$ by Svitlyk *et al* show a similar irreversibility in the temperature variation of several structural parameters, most notably the Se height [34].

3.3. Order/disorder in the $TlFe_{2-z}S_2$ sulphides with different z

In order to investigate the effect of the Fe content, z on the vacancy and magnetic ordering in $TlFe_{2-z}S_2$ sulphides, a second sample with the nominal composition $TlFe_{1.5}S_2$ was synthesized using the synthetic route described earlier. Powder
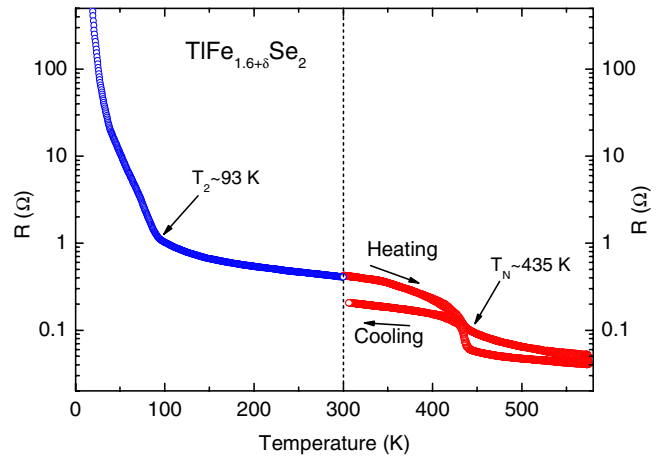

Figure 8. Low and high temperature dependence of the electrical resistance of $TlFe_{1.6+\delta}Se_2$ in zero field. The anomaly observed at T_2 is related to the spin re-orientation of the iron magnetic moments.

XRD data revealed that the $TlFe_{1.5}S_2$ sample consisted of a mixture of two phases: the *I4/mmm* tetragonal structure and an orthorhombic superstructure with a $\sqrt{2}\,a\times2\sqrt{2}\,a\times c$ cell (space group *Ibam*), derived from the original *I4/mmm* lattice, which is only present if the iron deficiency is large, as reported earlier by Zabel *et al* in 1980 and Sabrowsky *et al* in 1986 [6, 35]. This was also observed in our previous $TlFe_{2-z}(Se_{1-x}S_x)_2$ series where the orthorhombic phase was more prevalent in the compounds with high z [20].

The presence of the orthorhombic phase was confirmed by TEM and EDS analysis performed on several crystallites of $TlFe_{1.5}S_2$ (figure 9). Reconstruction of the reciprocal space evidenced an orthorhombic unit cell with the cell parameters $a \approx 5.4$ Å, $b \approx 10.5$ Å, $c \approx 13.3$ Å, in agreement with the Rietveld refinements of the powder XRD data ($a = 5.4004(3)$ Å, $b = 10.8518(7)$ Å and $c = 13.302(1)$ Å). The reflection conditions (hkl: $h + k + l = 2n$, $0kl$: $k = 2n$, ($l = 2n$), $hk0$: ($h + k = 2n$)) are compatible with the orthorhombic space group *Ibam* (n °72) and the average cationic composition of $TlFe_{1.4(1)}S_2$ is also consistent with the XRD Rietveld refinement results ($TlFe_{1.37(2)}S_2$).

The absence of any superstructure reflections in the laboratory XRD data would imply disordered iron vacancies in the iron plane in the tetragonal $a \times a \times c$ *I4/mmm* phase. However, in the NPD pattern collected at 300 K, both the (110) super lattice peak and the (101) magnetic peak are clearly visible (figure 10(*a*)). This indicates that the same $\sqrt{5}\,a\times\sqrt{5}\,a\times c$ lattice found in the pure selenide $TlFe_{1.6+\delta}Se_2$ is also present in the $TlFe_{1.5}S_2$ sample and that the signal-to-noise ratio in the XRD data is too low to detect the superstructure reflections. The long-range AFM order shown here demonstrates that at least a significant proportion of the $\sqrt{5}\,a\times\sqrt{5}\,a\times c$ lattice is perfectly ordered with the stoichiometry $TlFe_{1.6}S_2$ (i.e. empty Fe2 sites). The resulting magnetic moment of $1.0(1)$ μ_B at 300 K for $TlFe_{1.5}S_2$ is almost half of that of the pure selenide, $1.82(5)$ μ_B. The variation of the intensity of the (101) magnetic peak with temperature for $TlFe_{1.5}S_2$ is shown in the inset of figure 10(*a*). Just as for the partially S substituted $TlFe_{1.75}(Se_{0.65}S_{0.35})_2$ sample (figure 4(*c*)) there is a saturation of the magnetic moment at low temperature

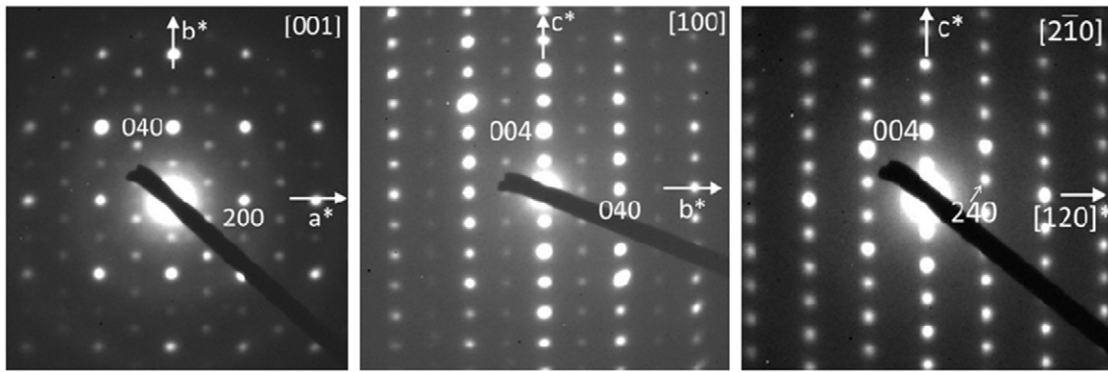**Figure 9.** Electron diffraction patterns of TlFe$_{1.5+\delta}$S$_2$ recorded along the [001], [100] and [2$\bar{1}$0] directions (left to right) indexed in an orthorhombic cell.

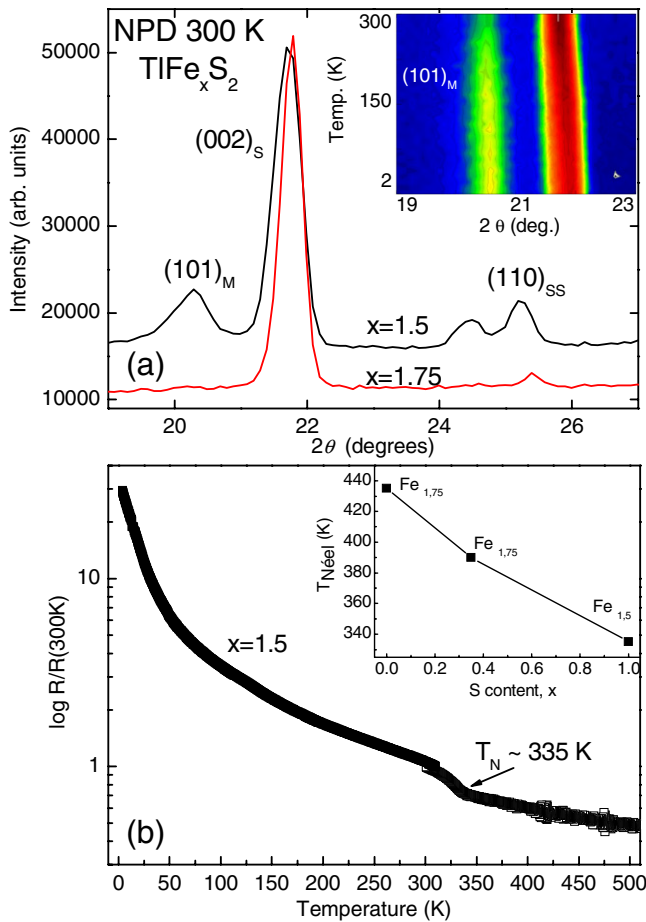**Figure 10.** (*a*) Selected low 2-theta region of the NPD patterns of TlFe$_{1.5}$S$_2$ and TlFe$_{1.75}$S$_2$ (nominal compositions) showing the (101) magnetic peak and the (110) super lattice peak related to the tetragonal $\sqrt{5}\,a \times \sqrt{5}\,a \times c$ cell. Inset: variation of the intensity of the (101) magnetic peak with temperature for the $x = 1.5$ sample. (*b*) Low- and high-temperature dependence of the electrical resistance of TlFe$_{1.5}$S$_2$ highlighting the signature of the long range AFM structure at T_N. Inset: the variation of T_N as a function of S content extracted from the resistivity data of the TlFe$_{2-z}$(Se$_{1-x}$S$_x$)$_2$ samples.

with a refined value of 1.8(1) μ_B at 1.5 K. This increase of the magnetic moment can also be seen in the relative ratio of the (101)$_M$/(002) peaks which is 0.63, 0.59 and 0.45 at 1.5, 150 and 300 K, respectively. Hence, the Fe magnetic moment remains high at low temperature for both the

S-substituted samples (2.21(9) μ_B and 1.8(1) μ_B at 1.5 K for $x = 0.35$ and 1, respectively) meaning that introducing S into the system does not strongly affect the magnetic properties (inset figure 7(*c*)) over the whole range of substitution. This is one explanation as to why superconductivity is absent in the TlFe$_{1.6+\delta}$(Se$_{1-x}$S$_x$)$_2$ series.

Figure 10(*b*) shows the electrical resistance (R(T)) behaviour of polycrystalline TlFe$_{1.5}$S$_2$. There is a clear kink in the curve around $T_N \sim 335$ K, confirming the existence of long-range magnetic order in the associated $\sqrt{5}\,a \times \sqrt{5}\,a \times c$ lattice. A similar transition temperature was observed in our previous Tl$_{0.8}$Fe$_{1.5}$S$_2$ (nominal composition) powder sample, $T_N \sim 334$ K [20]. The variation of the Neel temperature, T_N, (extracted from the R(T) curves) with increased S content (x) for TlFe$_{2-z}$(Se$_{1-x}$S$_x$)$_2$ is plotted in the inset of figure 10(*b*).

In the first part of this study we observed that sulphur rich compositions produce an increased iron occupation on the (empty) Fe2 sites (inset figure 5(*c*)), preventing the magnetic ordering in the $\sqrt{5}\,a \times \sqrt{5}\,a$ iron plane for $x > 0.35$. Here we demonstrate that reducing the nominal iron content of the mixture permits a stabilization of this $\sqrt{5}\,a \times \sqrt{5}\,a \times c$ AFM phase in rich S compositions. The choice of the nominal Fe content is therefore a crucial parameter. In the case of thallium selenides, May *et al* have shown that different growth conditions i.e. different nominal TlFe$_x$Se$_2$ composition, produce crystals with very different magnetization behaviour related to its micro-structure consisting of nano-scale domains of ordered and disordered iron vacancy regions with different relative proportion [32].

4. Conclusions

The isovalent substitution of S for Se in the TlFe$_{1.6+\delta}$(Se$_{1-x}$S$_x$)$_2$ system has been studied by neutron powder diffraction for the first time over the full range of $0 \le x \le 1$. Complementary XRD, electron diffraction using a TEM and transport measurements have also been performed. Our work shows the strong interplay between the existence of long range AFM magnetic order and crystallographic parameters. By carefully controlling the nominal iron content of the sample, we were able to stabilize the long-range 'block checkerboard' AFM order related to the $\sqrt{5}\,a \times \sqrt{5}\,a \times c$ superstructure for rich sulphur compositions

with the Néel temperature varying from 435 K ($x = 0$) down to 335 K ($x = 1$). At low temperature the iron magnetic moment remains high for all S compositions (from $x = 0$ to $x = 1$) and the magnetism is not strongly affected by the Se/S substitution. This is one important factor which contribute to explain why superconductivity is not induced in the TlFe$_{1.6+\delta}$(Se$_{1-x}$S$_x$)$_2$ system. However, for $x > 0.35$, keeping a too large iron content in the nominal mixture, results in compounds that are not magnetically ordered at RT, nor down to the lowest temperature of ~2 K (as measured by NPD), because the Fe2 sites of iron vacancies become filled and the vacancy ordering is lost.

Acknowledgments

References

[1] Guo J, Jin S, Wang G, Wang S, Zhu K, Zhou T, He M and Chen X 2010 *Phys. Rev.* B **82** 180520
[2] Wang A F *et al* 2011 *Phys. Rev.* B **83** 060512
[3] Shermadini Z *et al* 2011 *Phys. Rev. Lett.* **106** 117602
[4] Fang M, Wang H, Dong C, Li Z, Feng C, Chen J and Yuan H Q 2011 *Eur. Phys. Lett.* **94** 27009
[5] Häggström L, Verma H R, Bjarman S, Wäppling R and Berger R 1986 *J. Solid State Chem.* **63** 401
[6] Sabrowsky H, Rosenberg M, Welz D, Deppe P and Schäfer W 1986 *J. Magn. Magn. Mater.* **54** 1497
[7] Sales B C, McGuire M A, May A F, Cao H, Chakoumakos B C and Sefat A S 2011 *Phys. Rev.* B **83** 224510
[8] Yu R, Zhu J-X and Si Q 2011 *Phys. Rev. Lett.* **106** 186401
[9] Yan X W, Gao M, Lu Z Y and Xiang T 2011 *Phys. Rev. Lett.* **106** 087005
[10] Texier Y, Deisenhofer J, Tsurkan V, Loidl A, Inosov D S, Friemel G and Bobroff J 2012 *Phys. Rev. Lett.* **108** 237002
[11] Ding X *et al* 2013 *Nat. Commun.* **4** 1897
[12] Li W *et al* 2012 *Nat. Phys.* **8** 126
[13] Han F, Yang H, Shen B, Wang Z Y, Li C H and Wen H H 2012 *Phil. Mag.* **92** 2553
[14] Chen F *et al* 2011 *Phys. Rev.* X **1** 021020
[15] Kasahara S *et al* 2010 *Phys. Rev.* B **81** 184519
[16] Jiang S, Xing H, Xuan G F, Wang C, Ren Z, Feng C M, Dai J H, Xu Z A and Cao G H 2009 *J. Phys.:Condens. Matter* **21** 382203
[17] Yeh K W *et al* 2008 *Eur. Phys. Lett.* **84** 37002
[18] Mizuguchi Y, Tomioka F, Tsuda S, Yamaguchi T and Takano Y 2009 *Appl. Phys. Lett.* **93** 152505
[19] Lei H, Abeykoon M, Bozin E, Wang K, Warren J B and Petrovic C 2011 *Phys. Rev. Lett.* **107** 137002
[20] Toulemonde P, Santos-Cottin D, Lepoittevin Ch, Strobel P and Marcus J 2013 *J. Phys.:Condens. Matter* **25** 075703
[21] Klein T *et al* 2010 *Phys. Rev.* B **82** 184506
[22] Noat Y *et al* 2010 *J. Phys.:Condens. Matter* **22** 465701
[23] Rietveld H M 1969 *J. Appl. Crystallogr.* **2** 65
[24] Larson A C and Von Dreele R B 1994 *Los Alamos National Laboratory Report LAUR* 86-748
[25] Rodriguez-Carvajal J 1993 *Physica* B **192** 55
[26] Pomjakushin V *et al* 2011 *Phys. Rev.* B **83** 144410
[27] Wang Z, Song Y, Wang W Z, Chen Z, Tian H, Chen G, Guo J, Yang H and Li J 2011 *Phys. Rev.* B **83** 140505
[28] Ye F, Chi S, Bao W, Wang X F, Ying J J, Chen X H, Wang H D, Dong C H and Fang M 2011 *Phys. Rev. Lett.* **107** 137003
[29] Song Y J, Wang Z, Wang Z W, Hi H L, Chen Z, Tian H F, Chen G F, Yang H X and Li J Q 2011 *Eur. Phys. Lett.* **95** 37007
[30] Liu R H *et al* 2011 *Eur. Phys. Lett.* **94** 27008
[31] Bao W, Huang Q, Chen G F, Green M A, Wang D M, He J B, Wang X Q and Qiu Y 2011 *Chin. Phys. Lett.* **28** 086104
[32] May A F, McGuire M A, Cao H, Sergueev I, Cantoni C, Chakoumakos B C, Parker D S and Sales B C 2012 *Phys. Rev. Lett.* **109** 077003
[33] Cao H *et al* 2012 *Phys. Rev.* B **85** 054515
[34] Svitlyk V, Chernyshov E, Pomjakushina E, Krzton-Maziopa A, Conder K, Pomjakushin V and Dmitriev V 2011 *Inorg. Chem.* **50** 10703
[35] Zabel M and Range K J 1980 *Rev. Chim. Generale* **17** 561